ACS APPLIED MATERIALS & INTERFACES

Letter

www.acsami.org

Enhanced Charge Transport Kinetics in Anisotropic, Stratified Photoanodes

Nuri Yazdani,[†,‡] Deniz Bozyigit,[‡] Ivo Utke,[§] Jakob Buchheim,[†] Seul Ki Youn,[†] Jörg Patscheider,[⊥] Vanessa Wood,*[,‡] and Hyung Gyu Park*[,†]

[†]Nanoscience for Energy Technology and Sustainability, Department of Mechanical and Process Engineering, ETH Zürich,, Sonneggstrasse 3, Zürich CH-8092, Switzerland

[‡]Laboratory for Nanoelectronics, Department of Information Technology and Electrical Engineering, ETH Zürich, Gloriastrasse 35, Zürich CH-8092, Switzerland

[§]Laboratory for Mechanics of Materials and Nanostructures, EMPA, Feuerwerkstrasse 39, Thun CH-3602, Switzerland

[⊥]Laboratory for Nanoscale Materials Science, EMPA, Überlandstrasse 129, Dübendorf CH-8600, Switzerland

Supporting Information

ABSTRACT: The kinetics of charge transport in mesoporous photoanodes strongly constrains the design and power conversion efficiencies of dye sensitized solar cells (DSSCs). Here, we report a stratified photoanode design with enhanced kinetics achieved through the incorporation of a fast charge transport intermediary between the titania and charge collector. Proof of concept photoanodes demonstrate that the inclusion of the intermediary not only enhances effective diffusion coefficients but also significantly suppresses charge recombination, leading to diffusion lengths two orders of magnitude greater than in standard mesoporous titania photoanodes. The intermediary concept holds promise for higher-efficiency DSSCs.

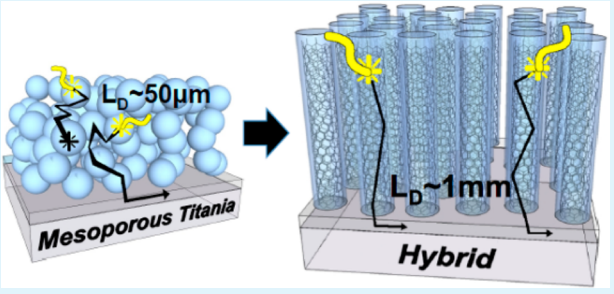

KEYWORDS: *dye-sensitized solar cells (DSSCs), photoanode, electron kinetics, carbon nanotubes*

The invention of dye-sensitized solar cells (DSSCs) marked an important advance in nanostructured solar cells design by leveraging different materials for the tasks of optical absorption and charge transport.[1] DSSCs have achieved efficiencies above 12%;[2] however, one remaining source of inefficiency in DSSCs is suboptimal charge transport through the mesoporous metal-oxide (e.g., titania) photoanodes.[3,4]

The photoinjected electron diffusion lengths of 30−60 μm observed for mesoporous titania photoanode-based DSSCs[5,6] place an upper limit on photoanode thickness, thereby limiting the areal absorption of the DSSC and the achievable short circuit current. Slow kinetics have also made it challenging to use lower redox potential electrolytes to achieve higher open circuit voltages as they also enhance recombination rates.[7−9]

Previous efforts to improve the charge transport kinetics through optimization and engineering of the photoanode include incorporation of highly conductive nanomaterials in the photoanode[10−14] and the use of vertically aligned titania nanotubes.[15−17] Although composite photoanodes of carbon nanotubes (CNTs) mixed with titania nanoparticles have shown shortened transport times owing to the high electron mobility in the CNTs, facile back transfer of electrons from the exposed surfaces of the CNTs to the electrolyte enhances recombination.[13] These composite photoanodes have therefore shown only small enhancements (on the order of a few micrometers) to the diffusion length.[11,13] Aligned titania nanotube-based photoanodes have demonstrated order of magnitude improvements in the diffusion length, primarily because of a large increase in the electron lifetime; however, the diffusion coefficients remained similar.[17] These results indicate that the improved electron kinetics comes from the reduced surface to volume ratio of the nanotube photoanodes compared to the nanoparticle photoanodes rather than a reduction in the tortuosity due to the vertically aligned nature of the photoanodes.

Here, we demonstrate, first in theory and then experimentally, that by including an intermediate layer between the titania and the current collector it is possible to enhance both the effective diffusion coefficients and recombination times in a photoanode. The intermediary must satisfy several conditions. First, the intermediary material should have a high electron mobility compared to titania. Second, photoinjected electrons should preferentially occupy states on the intermediary rather than the titania, which can be accomplished by utilizing a material with a high work function. Lastly, the photoanodes should be stratified such that the intermediary is physically

Received: December 27, 2013
Accepted: January 27, 2014
Published: January 27, 2014

   dx.doi.org/10.1021/am405987t | ACS Appl. Mater. Interfaces 2014, 6, 1389−1393

separated from the electrolyte, strongly suppressing recombination of electrons directly from the intermediary to the electrolyte.

Under illumination, electrons are continuously injected into the conduction band of the titania from excited dye molecules adsorbed on the titania surface, increasing the quasi-Fermi level,[6] or equivalently generating an excess charge density in the titania, n, compared to dark, equilibrium conditions. At any given time, a large fraction, n_L, are trapped in localized states below the conduction band, while a small fraction, n_C, remain in the conduction band of the titania, such that $n = n_L + n_c$ where $n_L \gg n_c$. For mesoporous photoanodes, the transport kinetics can be accurately modeled by a one-dimensional continuity equation, which assumes that only the conduction band electrons, n_C, are able to diffuse or recombine:[5,6]

$$\frac{\partial n}{\partial t} = \phi(x) + D_c\frac{\partial^2 n_c}{\partial x^2} - \frac{n_c}{\tau_c} \quad (1)$$

Here x is the direction perpendicular to the charge collector, $\phi(x)$ describes electron injection, D_c is the diffusion coefficient for electrons in the conduction band, and τ_c is the lifetime of those electrons (recombination time) before they recombine with cations in the electrolyte. For the photoanodes with the intermediary, we can consider another population, n_I, of electrons occupying states on the intermediary such that $n = n_L + n_c + n_I$. The electrons on the intermediary diffuse, but do not recombine with the electrolyte. Electron transport is thus governed by

$$\frac{\partial n}{\partial t} = \phi(x) + D_c\frac{\partial^2 n_c}{\partial x^2} + D_I\frac{\partial^2 n_I}{\partial x^2} - \frac{n_c}{\tau_c} \quad (2)$$

As shown in the Supporting Information, eqs 1 and 2 can be recast in terms of small perturbation, Δn, to the steady-state charge density n

$$\frac{\partial \Delta n}{\partial t} = D_n\frac{\partial^2 \Delta n}{\partial x^2} - \frac{\Delta n}{\tau_n} \quad (3)$$

where for mesoporous titania (MT) photoanodes

$$\tau_{n,MT} = \frac{dn}{dn_c}\tau_c, \quad D_{n,MT} = \frac{\partial n_c}{\partial n}D_c, \quad (4)$$

whereas for the photoanodes with the intermediary (i.e., hybrid (H) photoanodes):

$$\tau_{n,H} = \frac{\partial n}{\partial n_c}\tau_c, \quad D_{n,H} = \frac{\partial n_c}{\partial n}D_c + \frac{\partial n_I}{\partial n}D_I. \quad (5)$$

The density-dependent effective diffusion coefficient, D_n, and recombination time, τ_n, can be determined from photocurrent and photovoltage transients from a small perturbation, Δn, as shown in detail in Supporting Information.[5,6] For mesoporous photoanodes the diffusion length is independent of the charge density and given by

$$L_{MT}^2 = D_{n,MT}\tau_{n,MT} = D_c\tau_c \quad (6)$$

For hybrid photoanodes, the diffusion length depends on the charge density

$$L_{n,H}^2 = D_{n,H}\tau_n = D_c\tau_c + \frac{\partial n_I/\partial n}{\partial n_c/\partial n}D_I\tau_c \quad (7)$$

It follows from eq 7 that if the diffusion in the intermediary (D_I) is large and carriers rapidly transfer from the titania to the intermediary ($n_I \gg n_c$), the diffusion length can be dramatically increased by inclusion of the intermediary.

We experimentally demonstrate the potential of this photoanode design concept using vertically aligned, multiwalled CNTs as a model intermediary due to their outstanding electronic transport properties.[18,19] We grow CNT arrays on silicon (Figure 1a) and transfer them to an FTO substrate via a polymethylmethacrylate-assisted stamping technique (Figure 1b).[20−22] The CNTs are then conformally coated with titania via atomic layer deposition (Figure 1c). Scanning electron microscopy (SEM) images in Figure 1 reveal that the CNT arrays maintain their alignment during the fabrication. A titania thickness of 15 ± 1 nm is determined by measurements of the coated and uncoated CNT diameters (Figure 2a). A continuous coating is indicated by X-ray photoelectron spectroscopy (XPS) analysis (Figure 2b), which shows suppression of the carbon peak following the titania coating. Furthermore, whereas CNTs can efficiently exchange charge with ions in the electrolyte, exemplified by their use as a counter electrode,[23,24] our titania coating of CNTs successfully prevents any significant back transfer of charge from the CNTs to the electrolyte, evidenced

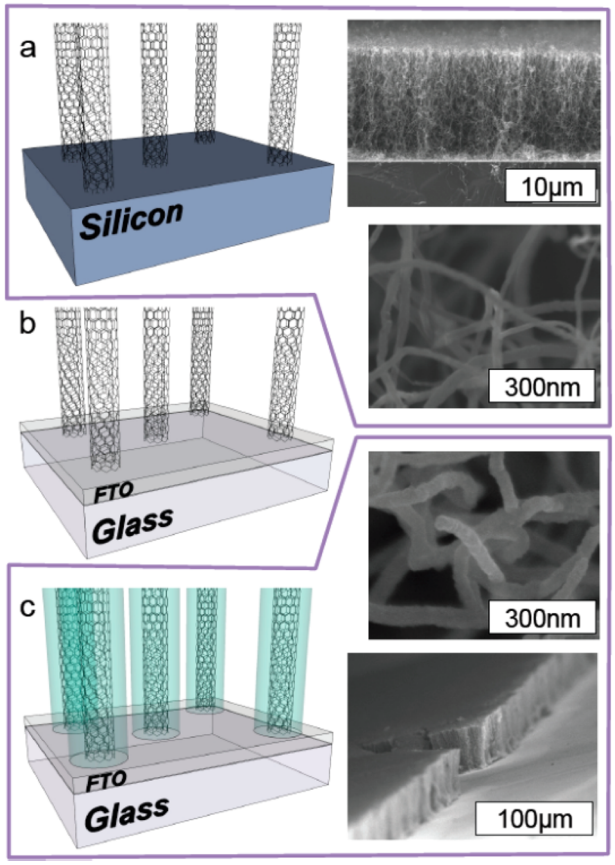

Figure 1. Process flow for fabricating a hybrid photoanode. (a) Vertically aligned CNTs are grown using atmospheric pressure chemical vapor deposition on a silicon wafer. (b) The CNT array is then transferred and affixed to an FTO substrate by a PMMA stamping procedure (see the Methods section). (c) CNTs of the transferred array are conformally coated with titania via atomic layer deposition (ALD). SEM images confirm the preservation of CNT vertical alignment after the transfer and ALD procedures.

dx.doi.org/10.1021/am405987t | ACS Appl. Mater. Interfaces 2014, 6, 1389−1393

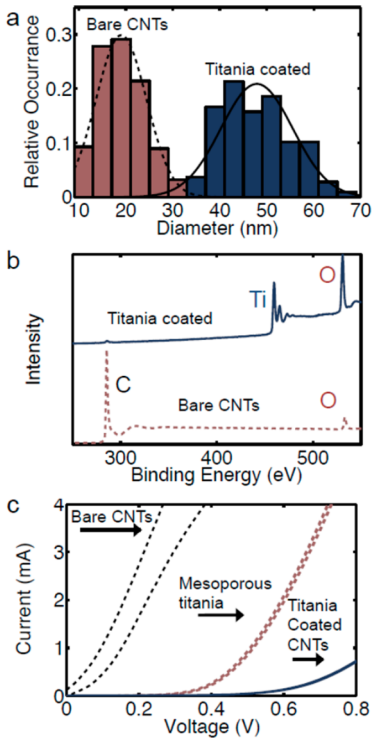

Figure 2. (a) Diameter histogram of the bare and titania-coated CNTs with Gaussian distribution fits revealing a titania thickness of 15.1 ± 0.2 nm. (b) XPS results of the bare and titania-coated CNTs. (c) Dark current–voltage measurements on completed electrochemical cells out of bare CNT-FTO anodes, mesoporous titania photoanodes, and hybrid photoanodes.

by current/voltage measurements on DSSCs made with bare and titania-coated CNT photoanodes (Figure 2c).

Figure 3a presents the current–voltage characteristics under AM1.5 illumination and in the dark for a DSSC incorporating our photoanode sensitized with *cis*-diisothiocyanato-bis(2,2′-bipyridyl-4,4′-dicarboxylato)-ruthenium(II)-bis-(tetrabutylammonium (Ruthenizer 535-bisTBA, Solaronix).

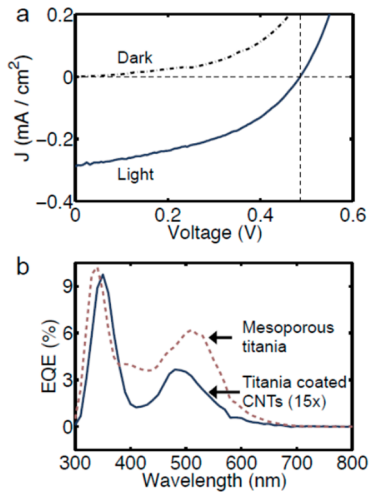

Figure 3. Characterization of hybrid photoanode in a DSSC. (a) Current–voltage characteristics of a DSSC based on the hybrid photoanode in dark (dashed) and under AM1.5 irradiation (solid). (b) External quantum efficiency (EQE) of the hybrid photoanode photoanode (with 15× scaling) and a mesoporous titania photoanode.

Although the open circuit voltages ~0.5 V are reasonable, the short circuit currents of the CNT-titania photoanodes are 50× smaller than that of high efficiency DSSCs.[2] This low current can be explained by the fact that the specific surface area (SSA) per volume of the CNT-titania photoanodes (1.1 (± 0.2) × 10^4 cm^2/cm^3) measured using focused ion beam (FIB) milling and SEM analysis (see the Supporting Information) is two orders of magnitude smaller than that of typical DSSCs (~1 × 10^6 cm^2/cm^3). The surface area determines the number of adsorbed dye molecules, and therefore the amount of absorbed light and the photocurrent. Furthermore, CNT samples exhibit 99.6–99.9% absorption for wavelengths between 200 and 1200 nm (see Figure S3 in the Supporting Information), which is another factor limiting the performance of the photoanode in the completed device. However, the external quantum efficiency (EQE) measurements on the CNT-titania photoanode DSSC (Figure 3b) show the same features as a DSSC with a mesoporous titania photoanode with two clear peaks at ~500 nm and in the UV, corresponding to the sensitizer at ~500 nm and absorption of the titania respectively. This indicates that the photons absorbed by the CNTs do not contribute to the photocurrent. The low EQE of our mesoporous titania reference DSSC compared to literature values is due to the use of a relatively thin titania layer (see the Supporting Information). We emphasize that our CNT-titania photoanode is intended as a demonstrator: although the particular selection of materials presents a limitation to solar cell performance, the photoanode functions as expected in a solar cell and exhibits the properties necessary to test our design concept for achieving longer diffusion lengths and slower recombination times via an intermediary.

The charge density of the photoanodes as a function of short circuit current/open circuit voltage are determined by integrating the transient which results from switching from an illuminated steady state condition, to an unilluminated short circuit condition. Measurements on the hybrid photoanode with the CNT intermediary in open and short circuit conditions are shown in Figure 4a. Small signal open circuit voltage and short circuit current transients for several baseline illumination conditions (steady state charge densities) are plotted in Figure 4b, c for the hybrid photoanode. The same measurements on mesoporous titantia photoanodes are shown in the Supporting Information.

In Figure 4d, D_n and τ_n are plotted as a function of charge density for both the mesoporous titantia and hybrid photoanodes. The D_n and τ_n values measured for the mesoporous photoanodes over the given range of charge densities are consistent with those reported in literature.[6] Over the range of charge densities measured, the effective diffusion coefficients for the hybrid photoanodes are nearly one order of magnitude greater than those of the mesoporous photoanodes, whereas the recombination times are enhanced by more than 2 orders of magnitude.

Another striking observation is that the open circuit charge densities of the hybrid photoanode are ~4 times larger compared to those of the mesoporous photoanode for similar open-circuit voltages (V_{OC} vs n is plotted for both photoanodes in Figure S5 in the Supporting Information). Charge extraction from the hybrid photoanodes remains very fast at the high electron densities found at open-circuit, as indicated by calculation of mean transport times shown in the Supporting Information (Figure S6). Therefore, although one cannot rule out that the CNTs also contribute a large portion of trap states

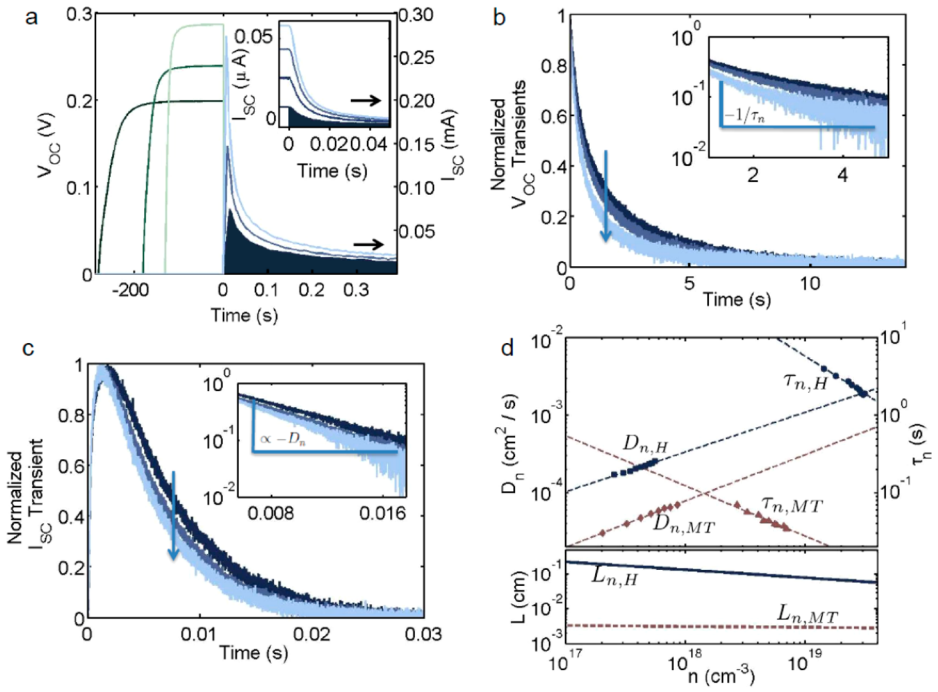

Figure 4. Results of the optoelectronic transient measurements. (a) Charge extraction measurements at various baseline illuminations for one of the hybrid photoanodes in an open circuit configuration. The inset shows several measurements for the same cell under short circuit conditions. The shaded region in both plots depicts the integral that gives the net charge in the photoanode at steady state (before $t = 0$ in these plots). (b) Plot of transients of the normalized open circuit voltage for different baseline illuminations of a hybrid photoanode, from which the recombination time, τ_n, can be extracted. The arrow indicates increasing baseline illumination. (c) Plot of transients of the normalized short circuit current for different baseline illuminations of a hybrid photoanode. The diffusion coefficients can be calculated by the time constants extracted from the transients as shown in the Supporting Information. The arrow indicates increasing baseline illumination. The insets in (b) and (c) show the decays of the transients on a log−linear scale, confirming that the transients can be fit with single exponentials. (d) Plot of the effective diffusion coefficient and recombination time as a function of charge density for the hybrid photoanodes (squares and circles, respectively) and mesoporous titania photoanodes (diamonds and triangles, respectively). The dotted lines show fits for the measured data. Shown below are the diffusion lengths as a function of charge density for the hybrid photoanodes (solid line) and the mesoporous titania photoanodes (dashed line) calculated using the fits to the diffusion coefficients and recombination times.

to the overall trap state density, we can rule out the possibility that trap states in the CNTs are the main cause of the very long recombination times. In other words, our assumption that the intermediary introduces states in which the electrons can diffuse, but not recombine, is confirmed.

For mesoporous titania photoanodes it has been observed that both $D_{n,\mathrm{MT}}$ and $\tau_{n,\mathrm{MT}}$ scale exponentially with the charge density n such that

$$D_{n,\mathrm{MT}} \propto n^{a-1},\ \tau_{n,\mathrm{MT}} \propto n^{1-a} \tag{8}$$

As summarized by Barnes et al.,[6] by modeling the trap states as an exponential distribution with a density of states ($g(E) \propto \exp[(E - E_c)/k_B T_0]$) the exponent a is given as $(mT/T_0)^{-1}$, where m compensates deviation of transport and recombination from ideality and T_0 is the characteristic temperature of the traps. Our measurements for the mesoporous photoanode yield $a = 1.62 \pm 0.02$. Combining eqs 4 and 8, we find $n_c \propto n^a$. An exponent $a > 1$ is consistent with our expectation that as n increases, more of the trap states of the titania are occupied such that a larger fraction of electrons will remain mobile in the conduction band of titania (n_c).

We also find that for the CNT-titania hybrid photoanode, $D_{n,\mathrm{H}}$ and $\tau_{n,\mathrm{H}}$ are both fit well with power laws over the range of charge densities measured. From the fit to the recombination times, we find that $\tau_{n,\mathrm{H}} \propto (\partial n_c/\partial n)^{-1} \propto n^{-0.97 \pm 0.04}$, which when plugged into eq 5 gives

$$D_{n,\mathrm{H}} = C_c n^{0.97\pm0.04} D_c + \frac{\partial n_I}{\partial n} D_I \tag{9}$$

where C_c is a constant. The fit to $D_{n,\mathrm{H}}$ in Figure 4d gives $D_{n,\mathrm{H}} \propto n^{0.60 \pm 0.02}$. Therefore, for eq 9 to hold, $n_I \propto n^{1.60 \pm 0.02}$ and $C_c D_c / C_I D_I \ll n^{0.6-0.97}$. For the range of charge densities n measured, this means that $C_c D_c / C_I D_I \ll 10^{-7}$. While we expect the diffusion coefficient in the CNTs to be greater than the diffusion coefficient in titania ($D_I > D_c$), a seven-order-of-magnitude difference is unrealistic, which implies that $C_c \ll C_I$. Thus, although the fraction n_c/n_I slowly increases with n, $n_c \ll n_I$, which indicates that photogenerated charge transfers rapidly from the titania to the intermediary as expected.

In the bottom half of Figure 4d, we plot the calculated diffusion lengths $L = (D_n \tau_n)^{1/2}$. A nearly constant diffusion length of around 30 μm is obtained for the mesoporous photoanode, whereas the diffusion length for the hybrid photoanode is charge-dependent and slowly decreases from >2 mm at 10^{17} cm^{-3} to ~1 mm at 1×10^{19} cm^{-3}. Although nonlinear recombination can lead to slight deviations from linearity of L in mesoporous photoanodes,[25] the strong nonlinearity of the diffusion length for the hybrid photoanode can be attributed in part to the increase in the fraction n_c/n_I.

In summary, we proposed a novel DSSC photoanode design with significantly enhanced electron kinetics as a result of an intermediary, which provides fast diffusion and slows recombination. The proof-of-concept CNT intermediary

confirmed the model predictions. Implementation of the design concept utilizing a low work-function, high electron mobility, but lightly absorbing intermediary should make it possible to achieve high efficiency DSSCs.

■ ASSOCIATED CONTENT

Supporting Information

Derivation of the small signal transient continuity equation as well as a detailed derivation of its solutions and how they can be related to measurements, description of the method to determine the volume fill fraction of the H photoanodes, a plot of the absorption coefficient for both types of photoanodes, plots of photocurrent and photovoltage transients for an MT photoanode, and a detailed account of the experimental methods as referred to in the text. This material is available free of charge via the Internet at http://pubs.acs.org.

■ AUTHOR INFORMATION

Corresponding Authors

*E-mail: vwood@ethz.ch.

*E-mail: parkh@ethz.ch.

Notes

The authors declare no competing financial interest.

■ ACKNOWLEDGMENTS

This research was partly funded by seed funding from the Materials Research Center of ETH Zürich and ETH Research Grant 42-12-2. The authors gratefully acknowledge support from the staff at the FIRST Center for Micro- and Nanoscience and the Binnig and Rohrer Nanotechnology Center. The authors thank Prof. David Norris for access to SEM.

■ REFERENCES

(1) O'Regan, B.; Grätzel, M. *Nature* **1991**, *353*, 24.

(2) Yella, A.; Lee, H. W.; Tsao, H. N.; Yi, C.; Chandiran, A. K.; Nazeeruddin, M. K.; Diau, E. W. G.; Yeh, C. Y.; Zakeeruddin, S. M.; Grätzel, M. *Science* **2011**, *334*, 629−634.

(3) Grätzel, M. *J. Photochem. Photobiol. C* **2003**, *4*, 145−153.

(4) Hagfeldt, A.; Boschloo, G.; Sun, L.; Kloo, L.; Pettersson, H. *Chem. Rev.* **2010**, *110*, 6595−6663.

(5) Bisquert, J.; Vikhrenko, V. S. *J. Phys. Chem. B* **2004**, *108*, 2313−2322.

(6) Barnes, P. R.; Miettunen, K.; Li, X.; Anderson, A. Y.; Bessho, T.; Gratzel, M.; O'Regan, B. C. *Adv. Mater.* **2013**, *25*, 1881−1922.

(7) Hamann, T. W. *Dalton Trans.* **2012**, *41*, 3111−3115.

(8) Yum, J.-H.; Baranoff, E.; Kessler, F.; Moehl, T.; Ahmad, S.; Bessho, T.; Marchioro, A.; Ghadiri, E.; Moser, J.-E.; Yi, C. *Nat. Commun.* **2012**, *3*, 631.

(9) Feldt, S. M.; Wang, G.; Boschloo, G.; Hagfeldt, A. *J. Phys. Chem. C* **2011**, *115*, 21500−21507.

(10) Tang, Y. B.; Lee, C. S.; Xu, J.; Liu, Z. T.; Chen, Z. H.; He, Z.; Cao, Y. L.; Yuan, G.; Song, H.; Chen, L. *ACS Nano* **2010**, *4*, 3482−3488.

(11) Yen, C. Y.; Lin, Y. F.; Liao, S. H.; Weng, C. C.; Huang, C. C.; Hsiao, Y. H.; Ma, C. C. M.; Chang, M. C.; Shao, H.; Tsai, M. C. *Nanotechnology* **2008**, *19*, 375305.

(12) Pint, C. L.; Takei, K.; Kapadia, R.; Zheng, M.; Ford, A. C.; Zhang, J.; Jamshidi, A.; Bardhan, R.; Urban, J. J.; Wu, M. *Adv. Energy Mater.* **2011**, *1* (6), 1040−1045.

(13) Chen, J.; Li, B.; Zheng, J.; Zhao, J.; Zhu, Z. *J. Phys. Chem. C* **2012**, *116*, 14848−14856.

(14) Kongkanand, A.; Martínez Domínguez, R.; Kamat, P. V. *Nano Lett.* **2007**, *7*, 676−680.

(15) Jennings, J. R.; Ghicov, A.; Peter, L. M.; Schmuki, P.; Walker, A. B. *J. Am. Chem. Soc.* **2008**, *130*, 13364−13372.

(16) Roy, P.; Kim, D.; Lee, K.; Spiecker, E.; Schmuki, P. *Nanoscale* **2010**, *2*, 45−59.

(17) Zhu, K.; Neale, N. R.; Miedaner, A.; Frank, A. J. *Nano Lett.* **2007**, *7*, 69−74.

(18) Baughman, R. H.; Zakhidov, A. A.; de Heer, W. A. *Science* **2002**, *297*, 787−792.

(19) Park, H. G.; Holt, J. K. *Energy Environ. Sci.* **2010**, *3*, 1028−1036.

(20) Jiao, L.; Fan, B.; Xian, X.; Wu, Z.; Zhang, J.; Liu, Z. *J. Am. Chem. Soc.* **2008**, *130*, 12612−12613.

(21) Lee, Y.; Bae, S.; Jang, H.; Jang, S.; Zhu, S.-E.; Sim, S. H.; Song, Y. I.; Hong, B. H.; Ahn, J.-H. *Nano Lett.* **2010**, *10*, 490−493.

(22) Reina, A.; Son, H.; Jiao, L.; Fan, B.; Dresselhaus, M. S.; Liu, Z.; Kong, J. *J. Phys. Chem. C* **2008**, *112*, 17741−17744.

(23) Li, S.; Luo, Y.; Lv, W.; Yu, W.; Wu, S.; Hou, P.; Yang, Q.; Meng, Q.; Liu, C.; Cheng, H. M. *Adv. Energy Mater.* **2011**, *1*, 486−490.

(24) Nam, J. G.; Park, Y. J.; Kim, B. S.; Lee, J. S. *Scr. Mater.* **2010**, *62*, 148−150.

(25) Bisquert, J.; Mora-Sero, I. *J. Phys. Chem. Lett.* **2010**, *1*, 450−456.